nature materials

ARTICLES

PUBLISHED ONLINE: 26 DECEMBER 2016 | DOI: 10.1038/NMAT4822

Designer vaccine nanodiscs for personalized cancer immunotherapy

Rui Kuai[1,2], Lukasz J. Ochyl[1,2], Keith S. Bahjat[3], Anna Schwendeman[1,2*†] and James J. Moon[1,2,4*†]

Despite the tremendous potential of peptide-based cancer vaccines, their efficacy has been limited in humans. Recent innovations in tumour exome sequencing have signalled the new era of personalized immunotherapy with patient-specific neoantigens, but a general methodology for stimulating strong CD8α$^+$ cytotoxic T-lymphocyte (CTL) responses remains lacking. Here we demonstrate that high-density lipoprotein-mimicking nanodiscs coupled with antigen (Ag) peptides and adjuvants can markedly improve Ag/adjuvant co-delivery to lymphoid organs and sustain Ag presentation on dendritic cells. Strikingly, nanodiscs elicited up to 47-fold greater frequencies of neoantigen-specific CTLs than soluble vaccines and even 31-fold greater than perhaps the strongest adjuvant in clinical trials (that is, CpG in Montanide). Moreover, multi-epitope vaccination generated broad-spectrum T-cell responses that potently inhibited tumour growth. Nanodiscs eliminated established MC-38 and B16F10 tumours when combined with anti-PD-1 and anti-CTLA-4 therapy. These findings represent a new powerful approach for cancer immunotherapy and suggest a general strategy for personalized nanomedicine.

Peptide-based cancer vaccines have been extensively investigated due to their good safety profiles and ease of manufacturing and quality control. However, their anti-tumour efficacy in clinical trials has been disappointing, a phenomenon that has been attributed to inefficient co-delivery of Ag peptides and adjuvants to draining lymph nodes (dLNs), and subsequent immunological tolerance and CTL fratricide[1]. Although depot-forming water-in-oil adjuvant systems can improve immunogenicity[2,3], booster immunizations can cause T-cell sequestration at the vaccine site, leading to T-cell exhaustion and deletion[4]. To address these issues, various nano-vaccine systems have been evaluated in animal models with varying degrees of success[5–15]. Despite the progress in the field, potential safety concerns and scale-up manufacturing of nanoparticles, especially in a manner suitable for personalized therapeutics with patient-specific neoantigens, still remain as the major challenges.

Here we propose an alternative, simple strategy where preformed nanocarriers, with an established clinical manufacturing procedure and excellent safety profiles in humans, are mixed with adjuvants and Ag peptides, including tumour-specific mutant neoepitopes[16–19], to produce personalized cancer vaccines (Fig. 1). Our strategy is based on synthetic high-density lipoprotein (sHDL) nanodiscs, composed of phospholipids and apolipoprotein A1 (ApoA1)-mimetic peptides. Compared with other HDLs containing 243-amino-acid ApoA1 purified from human plasma or produced recombinantly[20–22], sHDL nanodiscs are synthesized with 22-amino-acid ApoA1 mimetic peptide (22A), derived from the repeat α-helix domain of ApoA1[23], with no sequence homology to endogenous ApoA1, thus averting potential trigger of autoimmunity. Importantly, sHDL has been previously manufactured for clinical testing and proved to be safe in humans with the maximum tolerated dose at ~2.2 g m^{-2} (refs 24–26), a value one to two orders of magnitude greater than most polymeric or inorganic nanoparticles in clinical trials[27,28].

Here we set out to develop a nanodisc-based platform for neoantigen vaccination (Fig. 1). Exploiting the endogenous role of HDL as a nanocarrier for cholesterol, we modified a commonly used oligonucleotide containing the 5′-C-phosphate-G-3′ (CpG) motif, a potent Toll-like receptor-9 agonist, with cholesterol (Cho-CpG) to enhance its *in vivo* trafficking. We show that pre-formed sHDL nanodiscs can be simply mixed with cholesteryl-CpG and tumour Ag peptides, including neoantigens identified via tumour DNA sequencing, to produce homogeneous, stable, and ultrasmall nanodiscs in less than two hours at room temperature. The nanodiscs promote co-delivery of Ag/CpG to dLNs; prolong Ag presentation on antigen-presenting cells (APCs); elicit striking levels of broad-spectrum anti-tumour T-cell responses that significantly inhibit tumour growth; and eradicate established tumours when combined with immune checkpoint blockade. Based on the facile production process, robust therapeutic efficacy, and clinical safety demonstrated previously[24,25], our approach offers an attractive platform technology for patient-tailored cancer vaccines as well as other bioactive therapeutics.

Engineering nanodiscs for antigen and adjuvant delivery

We first identified lipids and peptides conducive to nanodisc formation. 1,2-dimyristoyl-*sn*-glycero-3-phosphocholine (DMPC) lipid films were hydrated and added with a series of ApoA1-mimetic peptides, followed by thermal cycling between 50 °C and 4 °C. We identified a subset of peptides, including 22A and D amino acids of 22A, that produced clear sHDL suspensions, stable for at least one month when stored at 4 °C (Supplementary Fig. 1a). In addition, use of phospholipids with transition temperature (T_m) below room temperature (for example, POPC and DOPC with $T_m = -2$ °C and −17 °C, respectively) produced murky liposomal suspensions, whereas lipids with high T_m (for example, DPPC and DMPC with $T_m = 41$ °C and 24 °C, respectively) formed clear sHDL suspensions

[1]Department of Pharmaceutical Sciences, University of Michigan, Ann Arbor, Michigan 48109, USA. [2]Biointerfaces Institute, University of Michigan, Ann Arbor, Michigan 48109, USA. [3]Discovery Research, Bristol-Myers Squibb Biologics Discovery California, Redwood City, California 94063, USA. [4]Department of Biomedical Engineering, University of Michigan, Ann Arbor, Michigan 48109, USA. †These authors contributed equally to this work. *e-mail: annaschw@umich.edu; moonjj@umich.edu

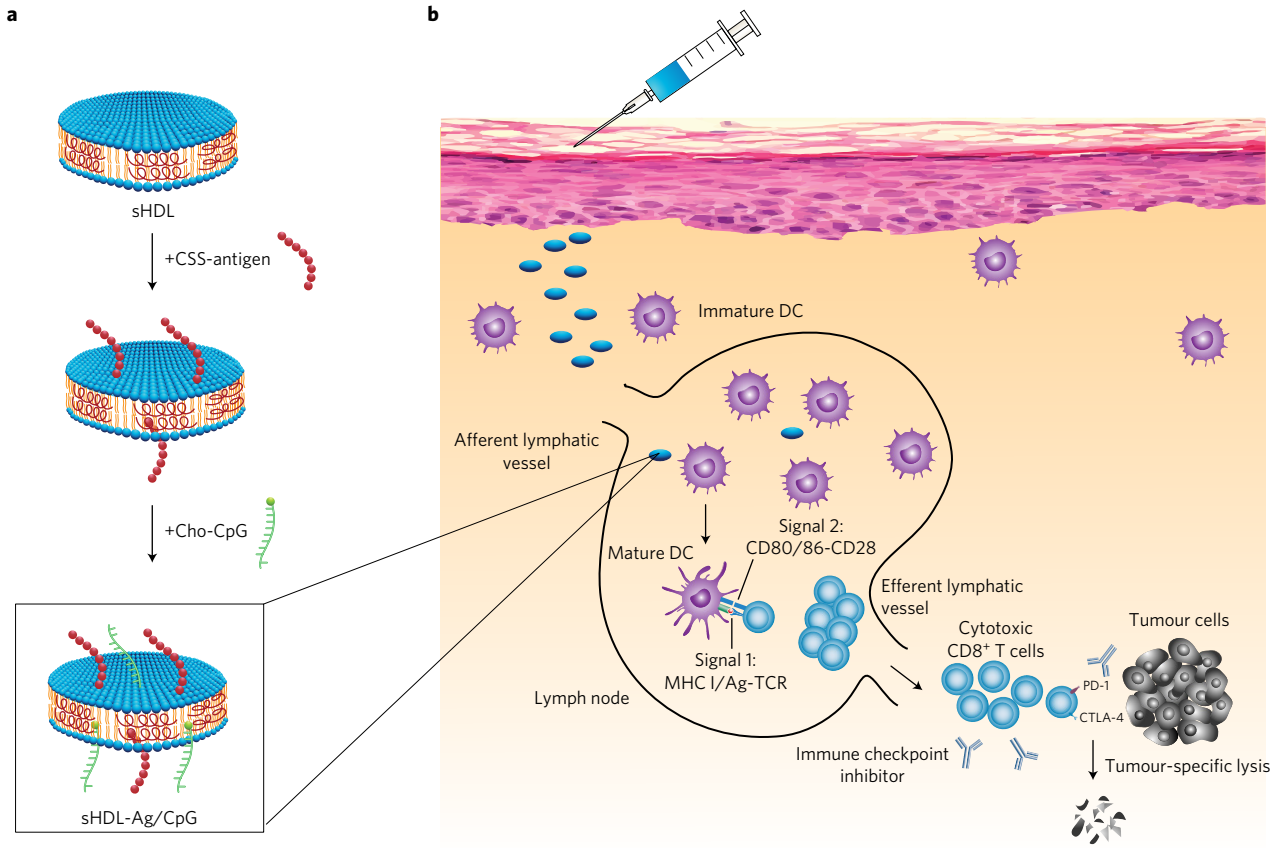

Figure 1 | Design of sHDL nanodisc platform for personalized cancer vaccines. a, sHDL nanodiscs, composed of phospholipids and apolipoprotein-1 mimetic peptides (22A), are engineered for co-delivery of antigen (Ag) peptides and adjuvants. Pre-formed sHDL nanodiscs displaying 4 mol% DOPE-PDP are mixed with cysteine-modified Ag peptides, including tumour-specific mutated neoantigens identified via tumour exome DNA sequencing, and subsequent incubation with cholesterol-modified immunostimulatory molecules (Cho-CpG) leads to formation of sHDL nanodiscs co-loaded with Ag and CpG (sHDL-Ag/CpG). **b**, Following administration, sHDL nanodiscs efficiently co-deliver Ag and CpG to draining lymph nodes, promote strong and durable Ag presentation by dendritic cells (DCs) (Signal 1), and induce DC maturation (Signal 2), resulting in elicitation of robust Ag-specific CD8α^+ cytotoxic T-lymphocyte (CTL) responses. Activated CTLs recognize and kill their target cancer cells in peripheral tissues and exert strong anti-tumour efficacy. Combination immunotherapy with immune checkpoint blockade further amplifies the potency of nanodisc vaccination, leading to elimination of established tumours.

in the presence of 22A (Supplementary Fig. 1b), showing flexibility in the materials design. On the basis of their size, homogeneity, and long-term stability, we chose to further investigate 22A and DMPC as the key components of nanodisc vaccines.

To achieve intracellular release of Ag within APCs via reduction-sensitive conjugation of Ag on sHDL, we synthesized dioleoyl-*sn*-glycero-3-phosphoethanolamine-*N*-[3-(2-pyridyldithio) propionate] (PDP, Supplementary Fig. 2) and incorporated PDP into sHDL (4 mol%). When incubated for 30 min at room temperature with Ag peptides modified with a cysteine-serine-serine (CSS) linker[29], sHDL nanodiscs were efficiently surface-decorated with various Ag peptides (for example, $OVA_{257-264}$, a model CD8α^+T-cell epitope Ag from ovalbumin; and Adgpk, neoantigen in MC-38 (ref. 16)), and subsequent incubation with Cho-CpG for 30 min at room temperature led to almost complete (~98%) insertion of CpG into sHDL, producing nanodiscs co-loaded with Ag and CpG (termed sHDL-Ag/CpG, with ~6.5 Ag peptides and ~1 CpG molecule per nanodisc, Supplementary Fig. 3 and Supplementary Table 1). sHDL-Ag/CpG exhibited uniform disc-like morphology with an average diameter of 10.5 ± 0.5 nm and polydispersity index of 0.20 ± 0.02 (Fig. 2a,b). Importantly, sHDL-Ag/CpG could be readily sterile-filtered and stored frozen at −20 °C for at least 8 weeks before thawing at 37 °C, without negatively affecting its homogeneity (Fig. 2c).

Sustained Ag presentation and cross-priming of T cells

We next examined the impact of nanodiscs on Ag presentation. Bone marrow-derived dendritic cells (BMDCs) pulsed for 24 h with sHDL-CSSSIINFEKL/CpG presented $OVA_{257-264}$ SIINFEKL with a greater efficiency than BMDCs treated with free Ag peptides admixed with CpG or sHDL-CSSSIINFEKL, as determined by staining DCs with the 25-D1.16 monoclonal antibody directed against SIINFEKL-H-2K^b complexes (Fig. 2d and Supplementary Fig. 4a,b). Interestingly, DCs pulsed with free SIINFEKL + CpG efficiently presented Ag for the first 6 h of incubation, but Ag presentation decreased precipitously past 6 h (Fig. 2e,f and Supplementary Fig. 4c), suggesting initial direct Ag binding to MHC-I molecules, followed by rapid Ag degradation or disassociation. In contrast, Ag presentation with sHDL-Ag/CpG gradually increased over time, achieving ~9-fold greater levels at 24 h and maintaining ~4-fold higher levels even at 48 h, compared with free SIINFEKL + CpG.

Intrigued by prolonged Ag presentation, we investigated the process of nanodisc uptake and Ag localization using $CSSSIINFEK_{(FITC)}L$; SIINFEKL modified with FITC at the ε-amino group in the lysine residue is known to retain its binding capacity to H-2K^b molecules[30]. JAWSII cells (immortalized immature DCs) incubated with free Ag(FITC) + CpG displayed weak fluorescence signal on the plasma membrane at 6 h, and only dim fluorescence was observed by 24 h (Fig. 2g and Supplementary Fig. 5). In stark

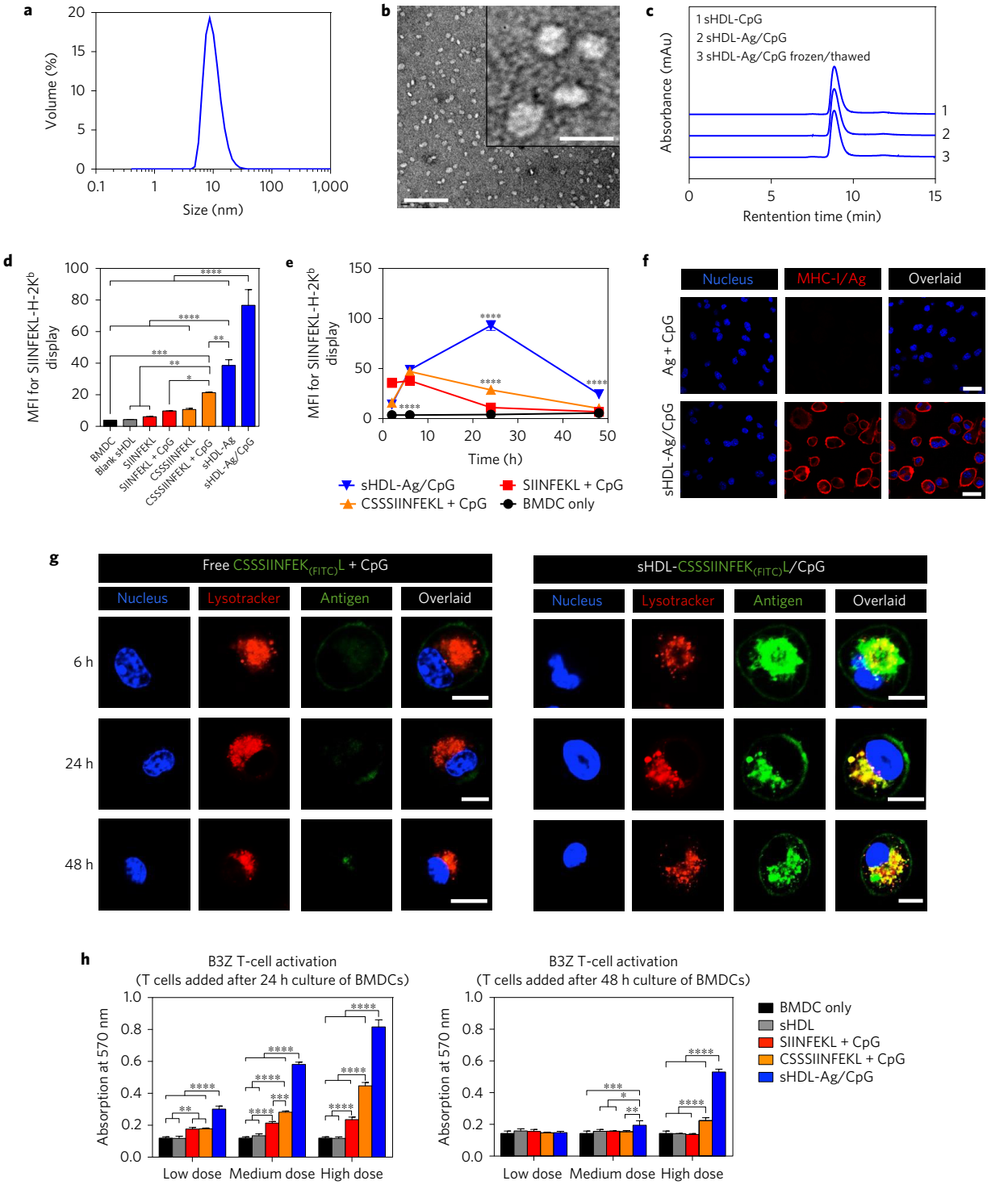

Figure 2 | Strong and durable Ag presentation mediated by sHDL nanodiscs. a,**b**, Dynamic light scattering analysis (**a**) and transmission electron microscopy imaging (**b**) showed uniform sHDL-Ag/CpG (10.5 nm ± 0.5 average diameter) with nanodisc-like morphology. Scale bar, 100 nm. Scale bar in the inset, 20 nm. **c**, Homogeneity of nanodiscs was maintained after sterile filtration (0.22 μm), and long-term storage (8 weeks) at −20 °C, followed by thawing at 37 °C. **d**,**e**, BMDCs were incubated with vaccine formulations for 24 h (**d**) or the indicated lengths of time (**e**), and Ag presentation was quantified by flow-cytometry analysis of DCs stained with 25-D1.16 monoclonal antibody that recognizes the SIINFEKL-H-2K^b complex. **f**,**g**, Confocal microscopy images of JAWSII cells (immature DCs). **f**, JAWSII cells were incubated with free Ag + CpG or sHDL-Ag/CpG for 24 h and stained with 25-D1.16 monoclonal antibody. Scale bars, 20 μm. **g**, JAWSII cells were incubated with free CSSSIINFEK$_{(FITC)}$L + CpG or sHDL-CSSSIINFEK$_{(FITC)}$L/CpG for 6, 24 or 48 h, followed by staining with Hoechst and Lysotracker. Scale bars, 10 μm. **h**, BMDCs were incubated with different concentrations of indicated formulations: low dose = 20 nM SIINFEKL and 3 nM CpG; medium dose = 100 nM SIINFEKL and 15 nM CpG; and high dose = 500 nM SIINFEKL and 75 nM CpG. After incubation for 24 h or 48 h, BMDCs were co-cultured with SIINFEKL-specific B3Z T-cell hybridoma for another 24 h, followed by assessment of T-cell activation. The data show mean ± s.d. from a representative experiment ($n = 3$) from 2–4 independent experiments. *$p < 0.05$, **$p < 0.01$, ***$p < 0.001$, and ****$p < 0.0001$, analysed by one-way (**d**) or two-way (**e**,**h**) ANOVA with Bonferroni multiple comparisons post-test.

contrast, sHDL-Ag(FITC)/CpG treatment led to strong FITC signal co-localized with endosomes/lysosomes by 6 h, and robust Ag(FITC) signal was detected on cell membranes by 24 h and sustained up to 48 h. In addition, nanodiscs containing Rh-PE or Texas Red-labelled-22A were predominantly found within endosomes/lysosomes, indicating cellular uptake of intact whole nanodiscs (Supplementary Fig. 6). To assess the impact of prolonged Ag presentation on T-cell cross-priming, we treated BMDCs with free Ag peptides + CpG or sHDL-Ag/CpG for 24 or 48 h, and then added SIINFEKL-specific, H-2K^{b}-restricted B3Z T-cell hybridomas. BMDCs pulsed with sHDL-Ag/CpG promoted strong B3Z T-cell activation even after 48 h incubation, whereas free Ag peptides + CpG induced minimal B3Z T-cell activation beyond the 24 h period (Fig. 2h). Moreover, sHDL-Ag/CpG potently stimulated DC maturation (Supplementary Fig. 7). Altogether, whereas free Ag peptide was rapidly loaded and dissociated from MHC-I molecules on cell membranes, nanodiscs facilitated intracellular delivery of Ag/CpG and mediated their sustained release within endosomes/lysosomes, thereby promoting durable Ag presentation, APC maturation, and cross-priming of CD8α^{+} T cells *in vitro*.

Elicitation of robust, long-lived T-cell responses *in vivo*

We next investigated the impact of nanodiscs on lymphatic delivery of Ag/CpG and induction of CD8α^{+} T-cell responses *in vivo*[5]. C57BL/6 mice injected subcutaneously at the tail base with 31 nmol free CSSSIINFEK$_{(FITC)}$L had minimal FITC signal in inguinal dLNs after 1 day (Fig. 3a), potentially due to systemic dissemination of small-molecular-weight Ag peptide or direct Ag binding on non-APCs at the injection site[1]. In contrast, the sHDL-Ag group exhibited markedly increased FITC signal in dLNs ($p < 0.01$, Fig. 3a), with Ag(FITC) and Cy5-tagged 22A co-localized within dLNs (Supplementary Fig. 8). Similarly, injection of 2.3 nmol Cy5-tagged Cho-CpG in sHDL increased its LN accumulation, compared with injection in free soluble form ($p < 0.01$, Fig. 3b). These results showed that sHDL nanodisc promoted co-delivery of Ag and CpG to dLNs. We next immunized C57BL/6 mice with 15.5 nmol Ag and 2.3 nmol CpG (non-fluorophore tagged), and peripheral blood was analysed for the frequency of SIINFEKL-MHC-I tetramer^{+} CD8α^{+} T cells. The mixture of free Ag peptides (SIINFEKL or CSSSIINFEKL) and CpG induced 1–3% Ag-specific CTLs after the third immunization (Fig. 3c,d). As the benchmark, we also vaccinated animals with the equivalent doses of Ag and CpG emulsified in water-in-oil Montanide, which is arguably one of the strongest adjuvant systems in clinical trials for peptide-based cancer vaccines[2,3,31,32]. Ag + CpG + Montanide elicited ~2% Ag-specific CTLs after priming; however, no further T-cell expansion was observed even after the third immunization, consistent with a recent study reporting dysfunction and deletion of high-avidity T cells after repeated immunizations with a depot-forming water-in-oil adjuvant[4]. In contrast, the sHDL-Ag/CpG group elicited a peak frequency of ~21% Ag-specific CD8α^{+} T cells after the third vaccination ($p < 0.0001$, Fig. 3c,d). We observed similar levels of peak Ag-specific CTL responses after sHDL-Ag/CpG vaccination with the dosing intervals of 1, 2 or 3 weeks (Supplementary Fig. 9). When challenged with 2×10^{5} B16OVA cells, mice immunized with sHDL-Ag/CpG had no detectable tumour masses up to 28 days, whereas mice immunized with free Ag peptides + CpG or Ag + CpG + Montanide all succumbed to tumours with marginal survival benefits (Fig. 3e and Supplementary Fig. 10). Importantly, throughout our studies, we did not observe any signs of toxicity, autoimmunity, nor immune responses directed against the ApoA1-mimetic peptide 22A in animals immunized multiple times with sHDL-Ag/CpG (Supplementary Fig. 11).

We sought to rule out the possibility that CSS-modified peptides or Cho-CpG dissociated from sHDL-Ag/CpG *in vivo* was responsible for the strong CTL responses. Introducing the CSS linker to SIINFEKL and replacing free CpG with Cho-CpG in free soluble form resulted in minimal T-cell responses, and the physical mixture of Ag, CpG and sHDL also elicited weak CTL responses (Fig. 3f). In contrast, sHDL-Ag/CpG nanodiscs drastically improved CD8α^{+} T-cell responses, eliciting remarkable 41-fold greater frequency of Ag-specific CD8α^{+} T cells than the CSSSINFEKL + Cho-CpG group (day 35, $p < 0.0001$), with CTLs primarily exhibiting CD44^{high}CD62L^{low} effector phenotype and robust IFN-γ^{+} ELISPOT responses (Fig. 3f,g and Supplementary Fig. 12). We also examined the durability of T-cell responses; after achieving their peak ~30% responses, animals still maintained 10% Ag-specific CD8α^{+} T cells at 2 months post the last vaccination (20-fold greater than the free Ag + CpG group, $p < 0.001$, Fig. 3h), and efficiently eliminated B16OVA cells inoculated intravenously (Fig. 3i), demonstrating long-lived protection against tumour challenge. In contrast, the soluble vaccine failed to protect animals against the intravenous B16OVA challenge.

Tumour regression by combination neoAg immunotherapy

To demonstrate the utility of our platform technology for vaccination against neoantigens, we first employed the murine MC-38 colon carcinoma model recently reported to harbour a single-epitope mutation within Adpgk protein (ASMTN**R**ELM → ASMTN**M**ELM), with the neo-epitope presented in MHC-I H-2D^{b} molecules[16]. We confirmed the Adpgk neoantigen mutation in MC-38 cells by sequencing complementary DNA (Fig. 4a and Supplementary Fig. 13) and synthesized sHDL-Adpgk/CpG by mixing nanodiscs with the neo-epitope modified with the CSS linker and Cho-CpG. C57BL/6 mice immunized with sHDL-Adpgk/CpG generated remarkable 47-fold and 31-fold greater frequencies of neoantigen-specific CTLs, compared with the soluble Adpgk + CpG and Adpgk + CpG + Montanide groups, respectively ($p < 0.0001$, Fig. 4b,c), with tumour-specific cytotoxicity against MC-38 target cells (Supplementary Fig. 14) and long-lived T-cell responses, as in the case of sHDL-SIINFEKL/CpG vaccination (Fig. 4d). To investigate the therapeutic efficacy of nanodisc vaccination, C57BL/6 mice were inoculated subcutaneously with 10^{5} MC-38 cells and treated with 15.5 nmol Adpgk and 2.3 nmol CpG (Fig. 4e). Therapeutic vaccination with sHDL-Adpgk/CpG induced polyfunctional IFN-γ^{+} and IFN-γ^{+} TNF-α^{+} Adpgk-specific CD8α^{+} T cells and substantially slowed MC-38 tumour growth (Fig. 4e), compared with the traditional soluble Adpgk + CpG vaccine. However, no tumour rejection was observed in either vaccine group, potentially due to immunosuppression within the tumour microenvironment, as we detected high expression levels of programmed cell death-1 (PD-1) and its ligand PD-L1 among tumour-infiltrating CD8α^{+} T cells and tumour cells, respectively (Supplementary Fig. 15). To block the immunosuppressive PD-1/PD-L1 pathway[33,34], we combined the vaccines with anti-PD-1 antibodies. Combination immunotherapy with sHDL-Adpgk/CpG and anti-PD-1 treatment generated robust neoantigen-specific CTL responses and led to complete tumour regression in ~88% mice (Fig. 4f and Supplementary Fig. 16), compared with ~25% rate of tumour regression in the soluble Adpgk + CpG + anti-PD-1 group. Notably, 100% of surviving mice rejected the subsequent re-challenge with MC-38 cells inoculated at the contralateral flank on day 70, indicating immunological memory against tumour recurrence (data not shown).

Multi-epitope T-cell responses with cocktail nanodiscs

Finally, we evaluated our nanodisc platform in a melanoma model with B16F10 cells, as they are highly aggressive, poorly immunogenic, and hence hard to treat with conventional cancer vaccines. To prevent tumour immune escape by loss of a single mutant allele[35], we sought to elicit broad-spectrum T-cell responses by employing multiple antigens (multiAgs), including recently reported B16F10 mutated neo-epitopes (MHC-I-restricted M27

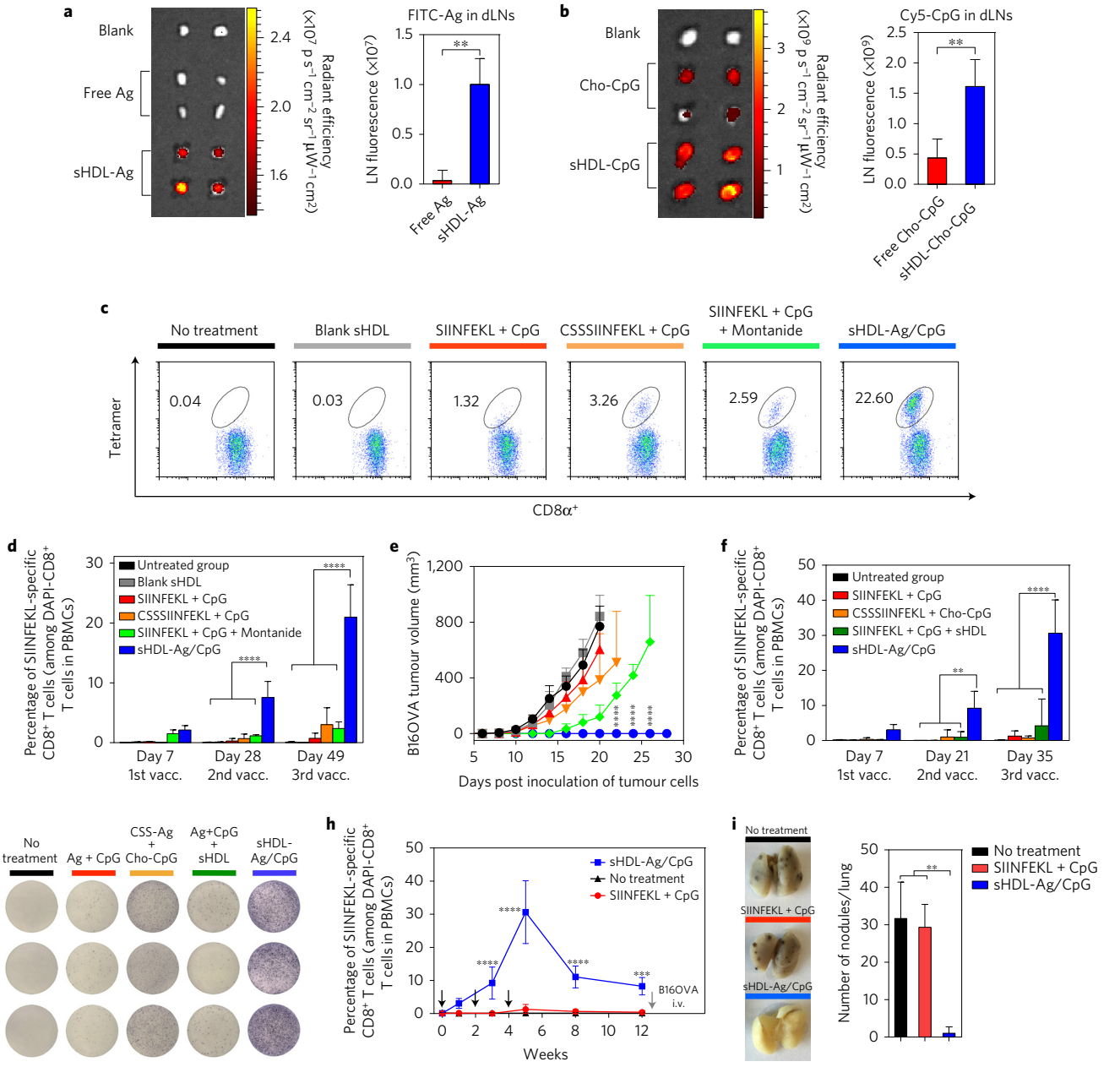

Figure 3 | Vaccine nanodiscs for LN-targeting of Ag and adjuvants and elicitation of CTL responses. a,**b**, C57BL/6 mice were administered subcutaneously at the tail base with 31 nmol FITC-tagged Ag (CSSSIINFEK$_{(FITC)}$L) (**a**) or 2.3 nmol Cho-CpG (20% labelled by Cy5) (**b**) in free soluble or sHDL form, and fluorescence signals in the draining inguinal LNs were quantified with IVIS after 24 h. **c**–**e**, C57BL/6 mice were immunized with the indicated formulations (15.5 nmol Ag peptide and 2.3 nmol CpG) on days 0, 21 and 42. Shown are their representative scatter plots on day 49 (**c**) and the frequency of SIINFEKL-specific CD8α$^+$ T cells in peripheral blood measured 7 days post each immunization by flow-cytometry analysis of tetramer$^+$ CD8α$^+$ T cells (**d**). **e**, On day 50, pre-vaccinated animals were challenged with subcutaneous flank injection of 2×10^5 B16OVA cells, and tumour growth was measured over time. **f**–**h**, C57BL/6 mice were immunized in a biweekly interval. Shown are percentage of SIINFEKL-specific CD8α$^+$ T cells in peripheral blood (**f**); ELISPOT analysis of IFN-γ spot-forming cells among splenocytes after *ex vivo* restimulation with SIINFEKL on day 35 (**g**); and Ag-specific CD8α$^+$ T-cell responses measured over 12 weeks post vaccination (black arrows indicate days of immunizations) (**h**). **i**, Vaccinated mice in **h** were intravenously challenged with 5×10^4 B16OVA cells two months after the third vaccination. Shown are pictures of the lungs and numbers of lung metastatic nodules counted on day 20 after the B16OVA challenge. The data show mean ± s.d. from a representative experiment ($n = 4$–5) from 2–3 independent experiments. $^{**}p < 0.01$, $^{***}p < 0.001$, and $^{****}p < 0.0001$, analysed by two-tailed unpaired Student's *t*-test (**a**,**b**), two-way ANOVA (**d**–**f**,**h**), or one-way ANOVA (**i**) with Bonferroni multiple comparisons post-test. Asterisks in **e** indicate statistically significant differences between sHDL-Ag/CpG and SIINFEKL + CpG + Montanide.

and MHC-II-restricted M30) as well as an MHC-I-restricted epitope from tyrosinase-related protein 2 (TRP2, a melanoma-associated Ag), all loaded in the same nanodiscs. C57BL/6 mice inoculated subcutaneously with 10^5 B16F10 cells were vaccinated with sHDL-multiAgs/CpG, eliciting a total of ~30% Ag-specific, IFN-γ$^+$ CD8α$^+$ and CD4$^+$ T cells in peripheral blood, compared with only 1–3% induced by the soluble multiAgs + CpG or multiAgs + CpG + Montanide groups ($p < 0.0001$, Fig. 5a and Supplementary Fig. 17). Vaccination with sHDL-multiAgs/CpG significantly inhibited B16F10 tumour growth, compared with the soluble or Montanide vaccines ($p < 0.0001$, Fig. 5b). Notably, removing either M27/M30 or TRP2 from sHDL-multiAgs/CpG compromised its

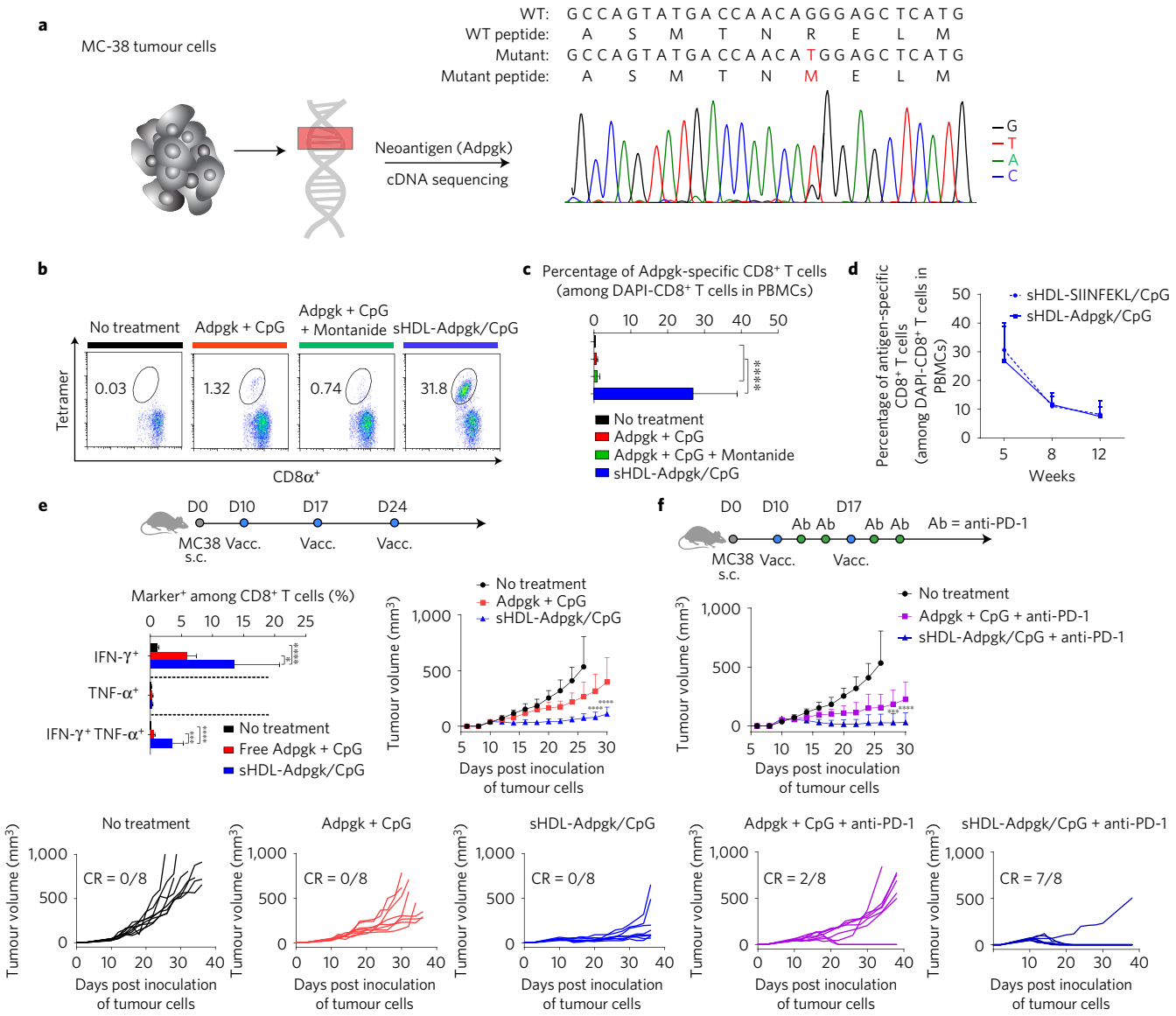

Figure 4 | Nanodisc-based neoantigen vaccination for personalized immunotherapy. a, Mutation of Adpgk in MC-38 murine colon adenocarcinoma cells was confirmed by sequencing cDNA of Adpgk. **b**–**d**, C57BL/6 mice were vaccinated three times with the indicated formulations (equivalent to 15.5 nmol mutated Adpgk peptide and 2.3 nmol CpG) in a biweekly interval, and the frequency of Adpgk-specific CD8α$^+$ T cells in peripheral blood was measured. Shown are the representative scatter plots (**b**), and the frequency of Adpgk-specific CTLs on day 35 (**c**). **d**, Clonal contraction of Ag-specific CD8α$^+$ T-cell responses elicited by sHDL-Adpgk/CpG and sHDL-SIINFEKL/CpG vaccines was monitored for eight weeks after the last vaccination. **e**, C57BL/6 mice were inoculated subcutaneously with 10^5 MC-38 tumour cells and vaccinated with the indicated formulations (equivalent to 15.5 nmol mutated Adpgk peptide and 2.3 nmol CpG) on days 10, 17 and 24. Shown are the percentages of intracellular IFN-γ$^+$, TNF-α$^+$, and IFN-γ$^+$TNF-α$^+$ CD8α$^+$ T cells in peripheral blood on day 30 after *ex vivo* restimulation with the mutated Adpgk Ag. Average and individual MC-38 tumour growth curves are shown with fraction of complete tumour regression (CR). **f**, C57BL/6 mice were inoculated subcutaneously with 10^5 MC-38 tumour cells and vaccinated with the indicated formulations (equivalent to 15.5 nmol mutated Adpgk peptide and 2.3 nmol CpG) on days 10 and 17. On days 1 and 4 after each vaccination, mice were administered intraperitoneally with anti-PD-1 (100 μg per mouse). Average and individual MC-38 tumour growth curves are shown. The data show mean ± s.d. from a representative experiment ($n = 5$–10) from 2–3 independent experiments. *$p < 0.05$, ***$p < 0.001$, and ****$p < 0.0001$, analysed by one-way ANOVA (**c**) or two-way ANOVA (**e**,**f**) with Bonferroni multiple comparisons post-test. Asterisks in **e**,**f** indicate statistically significant differences between sHDL-Ag/CpG and all other treatment groups.

therapeutic efficacy, suggesting the benefits of broad CTL responses against neoantigens and tumour-associated antigens (Fig. 5c). Lastly, we evaluated sHDL-multiAgs/CpG combined with dual immune checkpoint inhibitors. Combination immunotherapy with sHDL-multiAgs/CpG and anti-PD-1/anti-CTLA-4 treatment led to an impressive rate of B16F10 tumour rejection with ~90% of mice free of tumour, whereas the soluble multiAgs + CpG + anti-PD-1/anti-CTLA-4 treatment mediated tumour regression in ~38% of animals (Fig. 5d).

Overall, our results have significant clinical importance since these nanodiscs, with an established manufacturing procedure suited for neoantigen vaccination and excellent safety profiles in humans, can drastically improve co-delivery of antigens and adjuvants to LNs (Fig. 3a,b); sustain antigen presentation on DCs and cross-priming of T cells (Fig. 2e–h); drive multivalent CD8α$^+$ and CD4$^+$ T-cell immunity against neoantigens and tumour-associated antigens (Figs 3c–g and 4b–e and 5a) with long-term T-cell response (Fig. 3h,i); and significantly delay tumour

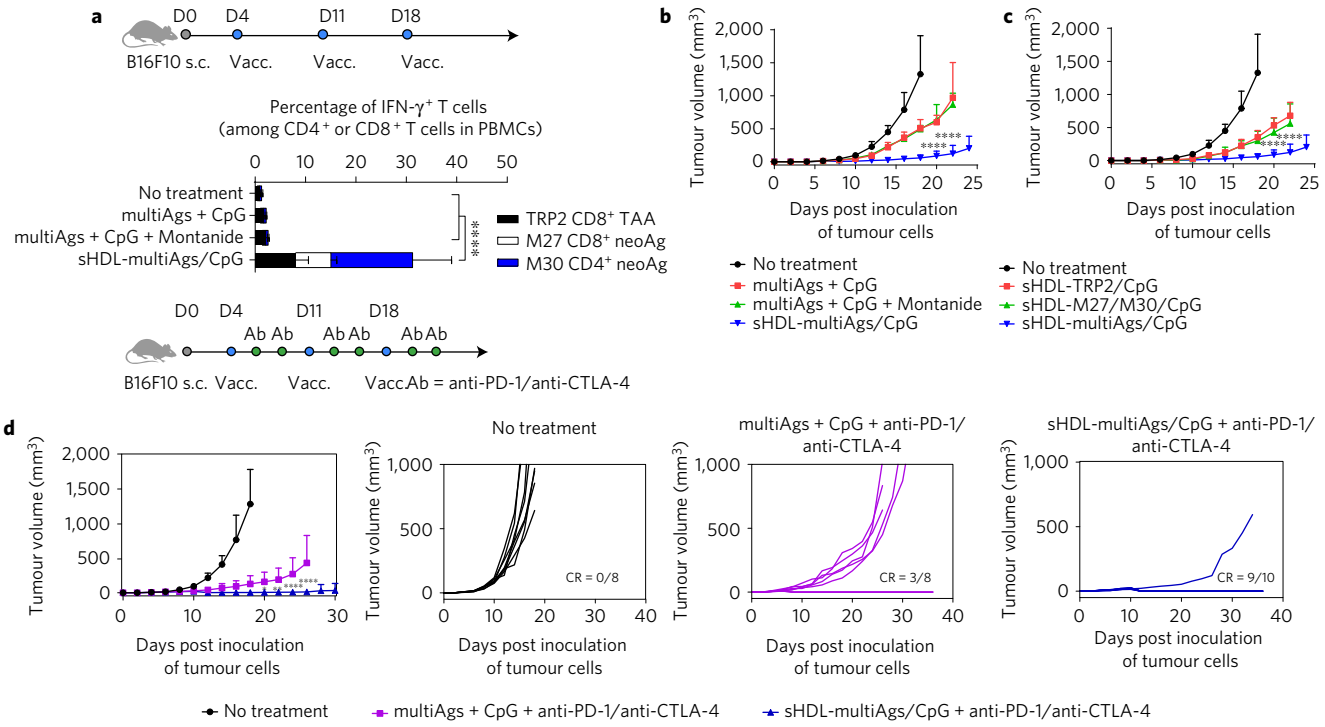

Figure 5 | Tumour eradication by combination immunotherapy with multi-epitope vaccine nanodiscs and immune checkpoint blockade. a–d, C57BL/6 mice were inoculated subcutaneously with 10^5 melanoma B16F10 cells and vaccinated on days 4, 11 and 18 with the indicated formulations (10 nmol of each antigen peptide and 2.3 nmol of CpG). For the combination immunotherapy, on days 1 and 4 after each vaccination, anti-PD-1 and anti-CTLA-4 (100 μg of each per mouse) were administered intraperitoneally. Shown are the percentage of IFN-γ^+ CD8α^+ or CD4$^+$ T cells in peripheral blood measured by intracellular cytokine staining (**a**), and average and individual B16F10 tumour growth curves (**b–d**). The data show mean ± s.d. from a representative experiment ($n = 5$–10) from 2–3 independent experiments. $^*p < 0.05$, $^{**}p < 0.01$, and $^{****}p < 0.0001$, analysed by one-way ANOVA (**a**) or two-way ANOVA (**b–d**) with Bonferroni multiple comparisons post-test. Asterisks in **b–d** indicate statistically significant differences between sHDL-Ag/CpG and all other treatment groups.

growth in the setting of therapeutic vaccination (Figs 4e and 5b,c). However, despite strong anti-tumour T-cell responses, nanodiscs administered as a monotherapy failed to eliminate tumours, possibly due to the immunosuppressive PD-L1/PD-1 pathway within the tumour microenvironment (Supplementary Fig. 15). Aiming to unleash the full cytotoxic potential of T cells[33,34], we combined nanodisc vaccination with immune checkpoint inhibitors, achieving potently amplified therapeutic efficacy and eradication of MC-38 and B16F10 tumours in >85% of animals (Figs 4f and 5d). Although other nanosystems in the literature[5–15] may be also applicable, this is, to the best of our knowledge, the first demonstration of anti-tumour efficacy with personalized nanomedicine tailored with tumour-specific neoantigen peptides.

While the work presented here provides the framework for future clinical translation, our strategy designed to generate neoantigen-specific cellular immunity requires tumour DNA/RNA exome sequencing, identification of neoantigens, and production of nanodiscs, followed by a multi-dose vaccine regimen, which collectively may protract the time window required for control of malignancies for late-stage patients. These issues may be tackled in the future by multi-pronged strategies that exploit combined immunotherapy targeted to humoral and innate arms of immunity[36] or radiation therapy[37] and select chemotherapeutics[38] known to delay tumour growth and synergize with T-cell vaccines.

In conclusion, we have developed a new nano-vaccine system ideally suited for individualized neo-epitope vaccination and demonstrated their potency to generate broad-spectrum T-cell responses with striking therapeutic efficacy when combined with immune checkpoint inhibitors. As the majority of somatic mutations in cancer cells are unique to each patient, cancer vaccines would require a personalized approach[16–19]. Coupled with the recent biomedical breakthroughs in neoantigen screening and immune checkpoint blockade[33,34,39–41], our approach may offer a powerful yet facile strategy for producing cancer vaccines designed for each patient. Furthermore, this platform technology may be generally applicable for personalized therapeutics with a wide range of bioactive molecules and imaging agents.

Methods

Methods, including statements of data availability and any associated accession codes and references, are available in the online version of this paper.

Received 24 September 2015; accepted 8 November 2016; published online 26 December 2016

References

1. Melief, C. J. & van der Burg, S. H. Immunotherapy of established (pre)malignant disease by synthetic long peptide vaccines. *Nat. Rev. Cancer* **8,** 351–360 (2008).
2. Speiser, D. E. *et al*. Rapid and strong human CD8$^+$ T cell responses to vaccination with peptide, IFA, and CpG oligodeoxynucleotide 7909. *J. Clin. Invest.* **115,** 739–746 (2005).
3. Fourcade, J. *et al*. Immunization with analog peptide in combination with CpG and montanide expands tumor antigen-specific CD8$^+$ T cells in melanoma patients. *J. Immunother.* **31,** 781–791 (2008).
4. Hailemichael, Y. *et al*. Persistent antigen at vaccination sites induces tumor-specific CD8$^+$ T cell sequestration, dysfunction and deletion. *Nat. Med.* **19,** 465–472 (2013).
5. Reddy, S. T. *et al*. Exploiting lymphatic transport and complement activation in nanoparticle vaccines. *Nat. Biotechnol.* **25,** 1159–1164 (2007).

6. Moon, J. J. *et al*. Interbilayer-crosslinked multilamellar vesicles as synthetic vaccines for potent humoral and cellular immune responses. *Nat. Mater.* **10,** 243–251 (2011).
7. Lee, I. H. *et al*. Imageable antigen-presenting gold nanoparticle vaccines for effective cancer immunotherapy *in vivo*. *Angew Chem. Int. Ed.* **51,** 8800–8805 (2012).
8. Li, A. V. *et al*. Generation of effector memory T cell-based mucosal and systemic immunity with pulmonary nanoparticle vaccination. *Sci. Transl. Med.* **5,** 204ra130 (2013).
9. Jeanbart, L. *et al*. Enhancing efficacy of anticancer vaccines by targeted delivery to tumor-draining lymph nodes. *Cancer Immunol. Res.* **2,** 436–447 (2014).
10. Xu, Z., Wang, Y., Zhang, L. & Huang, L. Nanoparticle-delivered transforming growth factor-beta siRNA enhances vaccination against advanced melanoma by modifying tumor microenvironment. *ACS Nano* **8,** 3636–3645 (2014).
11. Liu, H. *et al*. Structure-based programming of lymph-node targeting in molecular vaccines. *Nature* **507,** 519–522 (2014).
12. Rosalia, R. A. *et al*. CD40-targeted dendritic cell delivery of PLGA-nanoparticle vaccines induce potent anti-tumor responses. *Biomaterials* **40,** 88–97 (2015).
13. Chiu, Y. C., Gammon, J. M., Andorko, J. I., Tostanoski, L. H. & Jewell, C. M. Modular vaccine design using carrier-free capsules assembled from polyionic immune signals. *ACS Biomater. Sci. Eng.* **1,** 1200–1205 (2015).
14. Fan, Y. & Moon, J. J. Nanoparticle drug delivery systems designed to improve cancer vaccines and immunotherapy. *Vaccines* (*Basel*) **3,** 662–685 (2015).
15. Lizotte, P. H. *et al*. *In situ* vaccination with cowpea mosaic virus nanoparticles suppresses metastatic cancer. *Nat. Nanotech.* **13,** 295–303 (2016).
16. Yadav, M. *et al*. Predicting immunogenic tumour mutations by combining mass spectrometry and exome sequencing. *Nature* **515,** 572–576 (2014).
17. Kreiter, S. *et al*. Mutant MHC class II epitopes drive therapeutic immune responses to cancer. *Nature* **520,** 692–696 (2015).
18. Rajasagi, M. *et al*. Systematic identification of personal tumor-specific neoantigens in chronic lymphocytic leukemia. *Blood* **124,** 453–462 (2014).
19. Schumacher, T. N. & Schreiber, R. D. Neoantigens in cancer immunotherapy. *Science* **348,** 69–74 (2015).
20. Wolfrum, C. *et al*. Mechanisms and optimization of *in vivo* delivery of lipophilic siRNAs. *Nat. Biotechnol.* **25,** 1149–1157 (2007).
21. Fischer, N. O. *et al*. Colocalized delivery of adjuvant and antigen using nanolipoprotein particles enhances the immune response to recombinant antigens. *J. Am. Chem. Soc.* **135,** 2044–2047 (2013).
22. Duivenvoorden, R. *et al*. A statin-loaded reconstituted high-density lipoprotein nanoparticle inhibits atherosclerotic plaque inflammation. *Nat. Commun.* **5,** 3065 (2014).
23. Li, D., Gordon, S., Schwendeman, A. & Remaley, A. T. *Apolipoprotein Mimetics in the Management of Human Disease* 29–42 (Springer, 2015).
24. Khan, M., Lalwani, N., Drake, S., Crockatt, J. & Dasseux, J. Single-dose intravenous infusion of ETC-642, a 22-Mer ApoA-I analogue and phospholipids complex, elevates HDL-C in atherosclerosis patients. *Circulation* **108,** 563–564 (2003).
25. Miles, J. *et al*. Single-dose tolerability, pharmacokinetics, and cholesterol mobilization in HDL-C fraction following intravenous administration of ETC-642, a 22-mer ApoA-I analogue and phospholipids complex, in atherosclerosis patients. *Proc. Arterioscler. Thromb. Vasc. Biol.* **24,** E19 (2004).
26. Kuai, R., Li, D., Chen, Y. E., Moon, J. J. & Schwendeman, A. High-density lipoproteins: Nature's multifunctional nanoparticles. *ACS Nano* **10,** 3015–3041 (2016).
27. Alexis, F., Pridgen, E., Molnar, L. K. & Farokhzad, O. C. Factors affecting the clearance and biodistribution of polymeric nanoparticles. *Mol. Pharmacol.* **5,** 505–515 (2008).
28. Anselmo, A. C. & Mitragotri, S. A review of clinical translation of inorganic nanoparticles. *AAPS J.* **17,** 1041–1054 (2015).
29. Hirosue, S., Kourtis, I. C., van der Vlies, A. J., Hubbell, J. A. & Swartz, M. A. Antigen delivery to dendritic cells by poly(propylene sulfide) nanoparticles with disulfide conjugated peptides: cross-presentation and T cell activation. *Vaccine* **28,** 7897–7906 (2010).
30. Saini, S. K. *et al*. Dipeptides promote folding and peptide binding of MHC class I molecules. *Proc. Natl Acad. Sci. USA* **110,** 15383–15388 (2013).
31. US National Library of Medicine ClinicalTrials.gov [online] (2009); http://clinicaltrials.gov/show/NCT00819806 (Accessed 9 January 2015).
32. US National Library of Medicine ClinicalTrials.gov [online] (2008); http://clinicaltrials.gov/ct2/show/record/NCT00640861 (Accessed 9 January 2015).
33. Topalian, S. L. *et al*. Safety, activity, and immune correlates of anti-PD-1 antibody in cancer. *N. Engl. J. Med.* **366,** 2443–2454 (2012).
34. Zou, W., Wolchok, J. D. & Chen, L. PD-L1 (B7-H1) and PD-1 pathway blockade for cancer therapy: mechanisms, response biomarkers, and combinations. *Sci. Transl. Med.* **8,** 328rv324 (2016).
35. Verdegaal, E. M. *et al*. Neoantigen landscape dynamics during human melanoma–T cell interactions. *Nature* **536,** 91–95 (2016).
36. Moynihan, K. D. *et al*. Eradication of large established tumors in mice by combination immunotherapy that engages innate and adaptive immune responses. *Nat. Med.* http://dx.doi.org/10.1038/nm.4200 (2016).
37. Formenti, S. C. & Demaria, S. Combining radiotherapy and cancer immunotherapy: a paradigm shift. *J. Natl. Cancer Inst.* **105,** 256–265 (2013).
38. Kang, T. H. *et al*. Chemotherapy acts as an adjuvant to convert the tumor microenvironment into a highly permissive state for vaccination-induced antitumor immunity. *Cancer Res.* **73,** 2493–2504 (2013).
39. Gubin, M. M. *et al*. Checkpoint blockade cancer immunotherapy targets tumour-specific mutant antigens. *Nature* **515,** 577–581 (2014).
40. Robbins, P. F. *et al*. Mining exomic sequencing data to identify mutated antigens recognized by adoptively transferred tumor-reactive T cells. *Nat. Med.* **19,** 747–752 (2013).
41. Linnemann, C. *et al*. High-throughput epitope discovery reveals frequent recognition of neo-antigens by CD4+ T cells in human melanoma. *Nat. Med.* **21,** 81–85 (2015).

Acknowledgements

This work was supported in part by the NIH (R01GM113832, A.S.; R21NS091555, A.S.; UL1TR000433, J.J.M.; 1K22AI097291, J.J.M.; R01EB022563, J.J.M.; R01AI127070, J.J.M.), AHA (13SDG17230049, A.S.), UM MTRAC for Life Sciences (A.S.), and the UM College of Pharmacy faculty start-up fund (J.J.M., A.S.). J.J.M. is a Young Investigator supported by the Melanoma Research Alliance (348774), DoD/CDMRP Peer Reviewed Cancer Research Program (W81XWH-16-1-0369), and NSF CAREER Award (1553831). R.K. is supported by the Broomfield International Student Fellowship and the AHA Pre-doctoral Fellowship (15PRE25090050). L.J.O. is supported by pre-doctoral fellowships from UM Rackham and AFPE. We acknowledge J. Whitfield for his technical assistance with ELISPOT and thank R. H. Lyons, L. V. Diaz, J. K. Kim and P. H. Krebsbach for their contributions to cDNA sequencing. We acknowledge D. J. Irvine (MIT) and N. A. Kotov (UM) for critical review of the manuscript; the University of Michigan Consulting for Statistics, Computing, and Analytics Research (CSCAR) for help with statistical analyses; G. Skiniotis and A. Dosey (UM) for their aid with transmission electron microscopy; the NIH Tetramer Core Facility (contract HHSN272201300006C) for provision of MHC-I tetramers; N. Shastri (University of California, Berkeley) for B3Z T-cell hybridoma; K. Rock (University of Massachusetts, Amherst, Massachusetts) for B16OVA cells; and W. Zou (University of Michigan, Ann Arbor, Michigan) for MC-38 cells. Opinions interpretations, conclusions and recommendations are those of the authors and are not necessarily endorsed by the Department of Defense.

Author contributions

R.K., A.S. and J.J.M. designed the experiments. R.K. performed the experiments. L.J.O. contributed to the tetramer staining assays. R.K., A.S. and J.J.M. analysed the data and K.S.B. aided in the interpretation of data. R.K. and J.J.M. wrote the paper.

Additional information

Supplementary information is available in the online version of the paper. Reprints and permissions information is available online at www.nature.com/reprints. Correspondence and requests for materials should be addressed to A.S. or J.J.M.

Competing financial interests

A patent application for nanodisc vaccines has been filed, with J.J.M., A.S. and R.K. as inventors, and J.J.M. and A.S. are co-founders of EVOQ Therapeutics, LLC., that develops the nanodisc technology for vaccine applications.

Methods

Synthesis and characterization of sHDL nanodiscs. Dioleoyl-*sn*-glycero-3-phosphoethanolamine-*N*-[3-(2-pyridyldithio) propionate] (DOPE-PDP) was synthesized as reported previously[42]. DMPC and DOPE-PDP (molar ratio = 96:4) were dissolved in chloroform. The mixture was dried with nitrogen flow and placed under vacuum for at least 1 h. The resulting lipid film was hydrated in 10 mM sodium phosphate buffer and sonicated in a bath sonicator for 10 min, followed by probe sonication for another 2.5 min. ApoA1-mimetic peptide 22A dissolved in endotoxin-free water was added to the above mixture (22A/lipids = 1:7.5 molar ratio), which was then subjected to three heating and cooling cycles to obtain sHDL. To conjugate tumour antigen peptides to sHDL, cysteine-terminated tumour antigen peptides were added to the above sHDL (antigen peptide/DOPE-PDP = 2.5:1, molar ratio) and incubated at room temperature with gentle shaking on an orbital shaker. To construct sHDL nanodiscs with multi-antigens, each antigen peptide was reacted with DOPE-PDP (antigen peptide/DOPE-PDP = 1.5:1, molar ratio) for 1 h in dimethylformamide, which was removed by freeze-drying after dilution with endotoxin-free water. The lipid-peptide conjugates were added to pre-formed sHDL and incubated for 30 min at room temperature. Unreacted tumour antigen peptides were removed by using Zeba Spin Desalting columns (Pierce). Antigen peptides used in our studies include $OVA_{257-264}$SIINFEKL, CSSSIINFEKL, CSSSIINFEK(FITC)L, $TRP2_{180-188}$ SVYDFFVWL, CSVYDFFVWL, M27 neo-epitope LCPGNKYEM, M30 neo-epitope CSSVDWENVSPELNSTDQ, *Adpgk* mutant peptide ASMTNMELM (all obtained from GenScript), and CSSASMENMELM (from AnaSpec). The conjugation efficiency of tumour antigen peptides was calculated on the basis of the decrease of absorbance signal associated with DOPE-PDP as determined by HPLC. The loading efficiency of tumour antigen peptides in sHDL was confirmed by using FITC-labelled peptides and measuring the fluorescence intensity of sHDL formulations at Ex = 490 nm and Em = 520 nm after dissolving the formulations in PBS containing 1% Triton X-100. To load CpG in sHDL, different concentrations (0–200 μg ml^{-1}) of cholesterol-modified CpG 1826 (Cho-CpG, Integrated DNA Technologies) were incubated with sHDL at room temperature with gentle shaking on an orbital shaker. The amount of CpG incorporated into sHDL and free CpG was analysed by gel permeation chromatography (GPC) equipped with TSKgel G2000SWxl column (7.8 mm ID × 30 cm, Tosoh Bioscience LLC). The sHDL formulations were diluted to 0.5 mg ml^{-1} 22A with PBS, and the particle sizes were measured by dynamic light scattering (DLS, Zetasizer Nano ZSP). The morphology of sHDL was observed by transmission electron microscopy after proper dilution of the original samples with 1% uranyl acetate solution negative staining. All images were acquired on a JEM 1200EX electron microscope (JEOL USA) equipped with an AMT XR-60 digital camera (Advanced Microscopy Techniques).

BMDC activation, antigen presentation, and cross-priming. BMDCs were prepared as described previously[43]. Immature BMDCs were plated at 1×10^6 cells per well in 12-well plates. After 24 h, BMDCs were incubated with 75 nM CpG and/or 500 nM antigen peptide in various formulations or 0.5 μg ml^{-1} LPS (positive control) in complete media for different lengths of time (2, 6, 24 and 48 h) at 37 °C with 5% CO_2. BMDCs were harvested, washed with FACS buffer (1% BSA in PBS), incubated with anti-CD16/32 at room temperature, and then stained on ice with fluorophore-labelled antibodies against CD11c, CD40, CD80 and CD86, or PE-conjugated anti-mouse SIINFEKL/H-2K^b monoclonal antibody 25-D1.16 (eBioscience). Cells were then washed twice by FACS buffer, resuspended in 2 μg ml^{-1} DAPI solution, and analysed by flow cytometry (Cyan 5, Beckman Coulter). To assess cross-priming of T cells, BMDCs were incubated with different formulations of SIINFEKL (20, 100 and 500 nM) and CpG (3, 15 and 75 nM) for 24 h or 48 h at 37 °C. Cells were then carefully washed three times with PBS, and 10^5 B3Z CD8$^+$ T hybridoma cells (provided by N. Shastri) per well were added in RPMI 1640 supplemented with 10% FBS, 2 mM L-glutamine, 55 μM β-mercaptoethanol, 1 mM pyruvate, 100 U ml^{-1} penicillin and 100 μg ml^{-1} streptomycin. Throughout the studies, all cells were used as received and tested negative for mycoplasma contamination and rodent pathogens. After 24 h of incubation, the media were aspirated, and 150 μl CPRG/lysis buffer (0.15 mM chlorophenol red-β-D-galactopyranoside (CPRG), 0.1% Triton X-100, 9 mM $MgCl_2$, 100 μM mercaptoethanol in PBS) was added. The plates were incubated at 37 °C in the dark for 90 min, after which the absorbance of released chlorophenol red was measured at 570 nm using a microplate reader. To visualize intracellular distribution of nanodiscs, JAWSII cells (ATCC) were seeded at 1×10^6 cells on 35 mm Petri dishes (MatTek) and incubated with the physical mixture of free CSSSIINFEK(FITC)L and CpG, or sHDL-CSSSIINFEK(FITC)L/CpG for different lengths of time (6, 24 and 48 h). Cells were then washed three times with PBS and incubated for 30 min at 37 °C with 50 nM LysoTracker Red DND-99 (Invitrogen) and 2 μg ml^{-1} Hoechst in phenol/serum-free media to stain lysosomes and nuclei, respectively. In some studies, the lipid layers of sHDL were incorporated with 0.5 mol% DOPE-Rhod and 22A peptide of sHDL was labelled by incubating pre-formed sHDL with Texas Red-X succinimidyl ester (Life Technologies). JAWSII cells were then imaged using a confocal microscope (Nikon A1).

***In vivo* immunization and cancer immunotherapy studies.** Animals were cared for following federal, state, and local guidelines. All work performed on animals was in accordance with and approved by the University Committee on Use and Care of Animals (UCUCA) at the University of Michigan, Ann Arbor. Female C57BL/6 mice of age 6–8 weeks (Harlan Laboratories) were immunized with different formulations containing antigen peptides (15.5 nmol per mouse) and CpG (2.3 nmol per mouse) in 100 μl volume by subcutaneous injection at the tail base on indicated time points. In some studies, antigen peptide and CpG emulsified in Montanide served as a positive control. Briefly, antigen peptide (155 nmol) and CpG (23 nmol) in 0.5 ml PBS were thoroughly emulsified in 0.5 ml Montanide until the mixture was homogeneous and administered subcutaneously in 100 μl injection volume. For lymph node draining studies, C57BL/6 mice were injected with free CSSSIINFEK(FITC)L, sHDL-CSSSIINFEK(FITC)L, free Cho-CpG(Cy5), or sHDL-Cho-CpG(Cy5). After 24 h, inguinal lymph nodes were harvested, and FITC or Cy5 fluorescence signal was measured with an IVIS optical imaging system (Caliper Life Sciences). In some studies, induction of IgG response against 22A peptide was assessed by ELISA on immune sera as described previously[44]. The highest dilution with twice the absorbance of background was considered as the end-point dilution titre.

For prophylactic tumour challenge studies, vaccinated animals were challenged on day 8 after last immunization by subcutaneous injection of 2×10^5 B16OVA cells (provided by K. Rock) per mouse on the right flank. Tumour growth was monitored every other day, and the tumour volume throughout this study was calculated by the following equation[45]: tumour volume = length × width^2 × 0.52. Animals were euthanized when the tumour masses reached 1.5 cm in diameter or when animals became moribund with severe weight loss or ulceration. For the lung metastasis model, vaccinated animals were challenged by intravenous injection of 5×10^4 B16OVA cells per mouse, and lungs excised on day 20 were stained in Fekete's solution, followed by enumeration of B16OVA lung tumour nodules. For therapeutic tumour vaccination studies, C57BL/6 mice were inoculated with 1×10^5 MC-38 (provided by W. Zou) or B16F10 cells (ATCC) per mouse on the right flank by subcutaneous injection on day 0 and vaccinated on indicated days. For the combinatorial immunotherapy, anti-mouse PD-1 (100 μg per mouse, clone: RMP1-14, BioXcell) and/or anti-mouse CTLA-4 (100 μg per mouse, clone: 9D9, BioXcell) antibodies were administered intraperitoneally on days 1 and 4 after each vaccination. Tumour growth was monitored as indicated above.

Phenotypic and functional assessment of T cells. Immunized mice were analysed for the percentages of tumour antigen-specific CD8α$^+$ T cells using the tetramer staining assay as described previously[46,47] with peptide-MHC tetramer tagged with PE (for example, H-2K^b-restricted SIINFEKL (Beckman Coulter) or H-2D^b-restricted ASMTNMELM (the NIH Tetramer Core Facility)). CTL cytotoxicity was evaluated using the Lactate Dehydrogenase (LDH) Assay (CytoTox 96 Non-Radioactive Cytotoxicity Assay) *in vitro* with splenocytes from immunized mice and MC-38 target cells, as described previously[48,49]. ELISPOT assay was performed with splenocytes from immunized mice as described previously[50]. The intracellular cytokine staining assays on PBMCs were performed with anti-IFN-γ-PE and anti-TNF-α-FITC as described previously[6]. For analysis of tumour-infiltrating T cells, tumour tissues were excised at the indicated time points, cut into small pieces of 2–4 mm, and then placed in dissociation buffer (1 mg ml^{-1} of collagenase type IV and 0.1 mg ml^{-1} of DNase I in RPMI) for 30 min at 37 °C with gentle shaking. The cell suspension was passed through a 70-μm strainer, washed with FACS buffer, and stained with indicated antibodies, followed by flow cytometric analysis.

cDNA sequencing of neo-epitope (Adpgk) in MC-38 cells. Total RNA was extracted from MC-38 cells by the RNeasy mini Kit (QIAGEN) following the manufacturer's instructions. The first-strand cDNA was synthesized using 1 μg of total RNA with the SuperScript III First-Strand Synthesis SuperMix Kit (Invitrogen). Adpgk cDNAs with lengths of 250 bp and 485 bp were selectively amplified by using the following two sets of sequence-specific primers. Primer 1: 5′-TGCCAACCGCTTCATCTTCT-3′ (forward primer) and 5′-GGTAGACCAGC GTGTGGAAA-3′ (reverse primer); primer 2: 5′-CTCCAACGGGGCCATGAATA -3′ (forward primer) and 5′-CGTGGGAAAGACCTGCTGAT-3′ (reverse primer). The amplification was performed using the SuperScript One Step RT-PCR System (Invitrogen). The final cDNA products were visualized in 1.5% agarose gels with ethidium bromide, and the Adpgk cDNA bands were cut and purified using the PureLink Quick Gel Extraction and PCR Purification Combo Kit (Invitrogen). The purified cDNA was sequenced by the Sanger sequencing method at the University of Michigan DNA Sequencing Core.

Statistical analysis. Sample sizes were chosen on the basis of preliminary data from pilot experiments and previously published results in the literature. All animal studies were performed after randomization. Experiments were not performed in a blinded fashion. Data were analysed by one- or two-way analysis of variance (ANOVA), followed by Bonferroni *post hoc* test for comparison of multiple groups with Prism 5.0 (GraphPad Software). Data were normally distributed and variance

between groups was similar. *P* values less than 0.05 were considered statistically significant. All values are reported as means ± s.d. with the indicated sample size. No samples were excluded from analysis.

Data availability. All relevant data are available from the authors.

References

42. Kuai, R. *et al*. Efficient delivery of payload into tumor cells in a controlled manner by TAT and thiolytic cleavable PEG co-modified liposomes. *Mol. Pharmacol.* **7,** 1816–1826 (2010).
43. Lutz, M. B. *et al*. An advanced culture method for generating large quantities of highly pure dendritic cells from mouse bone marrow. *J. Immunol. Methods* **223,** 77–92 (1999).
44. DeMuth, P. C., Moon, J. J., Suh, H., Hammond, P. T. & Irvine, D. J. Releasable layer-by-layer assembly of stabilized lipid nanocapsules on microneedles for enhanced transcutaneous vaccine delivery. *ACS Nano* **6,** 8041–8051 (2012).
45. Gorrin-Rivas, M. J. *et al*. Mouse macrophage metalloelastase gene transfer into a murine melanoma suppresses primary tumor growth by halting angiogenesis. *Clin. Cancer Res.* **6,** 1647–1654 (2000).
46. Ochyl, L. J. & Moon, J. J. Whole-animal imaging and flow cytometric techniques for analysis of antigen-specific $CD8^+$ T cell responses after nanoparticle vaccination. *J. Vis. Exp.* **98,** e52771 (2015).
47. Fan, Y., Sahdev, P., Ochyl, L. J., J, J. A. & Moon, J. J. Cationic liposome-hyaluronic acid hybrid nanoparticles for intranasal vaccination with subunit antigens. *J. Control Release* **208,** 121–129 (2015).
48. Ning, N. *et al*. Cancer stem cell vaccination confers significant antitumor immunity. *Cancer Res.* **72,** 1853–1864 (2012).
49. Stephan, M. T., Moon, J. J., Um, S. H., Bershteyn, A. & Irvine, D. J. Therapeutic cell engineering with surface-conjugated synthetic nanoparticles. *Nat. Med.* **16,** 1035–1041 (2010).
50. Anthony, D. D. & Lehmann, P. V. T-cell epitope mapping using the ELISPOT approach. *Methods* **29,** 260–269 (2003).